IEEE Open Journal of
Antennas and Propagation

Received 31 December 2020; revised 31 January 2021; accepted 1 February 2021. Date of publication 18 February 2021; date of current version 16 March 2021.

Digital Object Identifier 10.1109/OJAP.2021.3059470

Scattering by Perfectly Conducting Cylindrical Targets Hidden Below a Multilayered Medium

CRISTINA PONTI [1,2] **(Member, IEEE)**

[1]Department of Engineering, "Roma Tre" University, 00146 Rome, Italy

[2]National Interuniversity Consortium for Telecommunications (CNIT), Unit of "Roma Tre" University, 00146 Roma, Italy

CORRESPONDING AUTHOR: C. PONTI (e-mail: cristina.ponti@uniroma3.it)

ABSTRACT An approach to solve the scattered field by perfectly conducting cylinders with circular cross-section, placed below a multilayered medium, under illumination by a line source, is presented. In principle, the interaction of the field scattered by the targets with the multilayer above leads to an infinite number of scattered fields, excited as multiple reflections in each layer by the interfaces. Nevertheless, the developed theoretical formulation is a very compact one, as only two scattered-field contributions are used in each layer, a down-propagating term, described as scattered-reflected field, and an up-propagating one relevant to the scattered-transmitted field. Suitable basis functions, i.e., cylindrical waves expressed through plane-wave spectra, are employed, which are defined through reflection and transmission coefficients of a multilayered medium. As shown in the numerical implementation, the method can be applied to the modeling of several radar problems of targets in complex environments. For example, the technique can be employed to model buried cylinders in geophysical scenarios, in Ground Penetrating Radar applications. The modeling of scattered field by hidden targets in Through-the-Wall radar surveys is another possible field of use. The multilayer may, indeed, model a stratified masonry, but also a room hiding a target in a buildings' interior.

INDEX TERMS Buried object detection, electromagnetic scattering, ground penetrating radar.

I. INTRODUCTION

MODELING of the electromagnetic scattering by cylinders placed below one or more dielectric layers is of interest in radar surveys of targets in complex environments. Applications are in the frame of Ground Penetrating Radar (GPR) [1]–[2], when the targets are buried in the subsoil, like, for example, in the fields of civil engineering or archeology. Furthermore, the proposed layout is compatible with scenarios of Through-the-Wall (TW) radar [4]–[5], employed in surveillance and rescue operation for the search of humans or objects hidden behind a wall. Several numerical/analytical techniques have been developed to solve the two-dimensional frequency-domain scattering by objects buried in a semi-infinite medium [6]–[15], mainly based on Greens' function or spectral approaches. The case of objects embedded in a layered medium has been considered in [16]–[19]. Objects are placed below one dielectric layer, in a semi-infinite medium, in [20]–[21]. In the literature, time-domain techniques are also employed, as the numerical results can give an interpretation of experimental data with pulsed GPRs [22]–[24]. In the numerical modeling of buried objects or targets in Through-the-Wall radar scenarios, Finite-Difference Time-Domain (FDTD) technique is used frequently to check the validity of imaging algorithms [25]–[27], as it is extremely flexible from the point of view of the layout of background media target shape. Use of time-domain results returns a qualitative imaging of the target, whereas a quantitative reconstruction, i.e., assessing its physical properties, makes use of frequency-domain data [28] and [29]. Therefore, in the case of synthetic data from the FDTD, they are preliminarily processed by a Fast Fourier Transform in order to extract the scattered field at the selected frequencies of the spectrum, used as input data to benchmark the inversion techniques [30]. In the field of Through-the-Wall radar, also Green's functions approaches have been proposed [31] and [32], and solved

under linearized inversion schemes for the imaging of the target. Benefits of modeling a multilayered background for applications to imaging techniques has been highlighted by many studies. In the subsurface analysis with the GPR, recent works [33] and [34] have proposed a stratified ground, as it represents a realistic modeling of practical backgrounds, and returns a more focused image of the target [35] and [36]. This work aims at providing a full-wave technique to solve the scattered field by targets below a multilayered medium in the frequency domain, which is accurate and fast, and possibly flexible in the modeling of the background environment. The proposed technique is semi-analytical, as the Cylindrical Wave Approach (CWA) [37]–[39] is applied, which makes use of sets of cylindrical waves as basis functions to express the scattered fields. The CWA has been applied to solve the scattering by perfectly conducting cylinders below one dielectric layer in [20], [21]. In [20], the scattered fields have been expressed as an infinite and convergent series of multiple scattered-reflected and scattered-transmitted field contributions, which describe the bounces excited by the two interfaces bounding each dielectric layers. The technique has been modified in [21], replacing the infinite series with a limited set of scattered fields, through a non-iterative approach which sums up all the multiple reflections through the use of suitable reflection and transmission coefficients. Here, the concept proposed in [21] is implemented to solve the interaction with a multilayer placed above the cylindrical targets. The formulation is extremely compact and efficient, and only two scattered fields are defined in each layer: a scattered-reflected field, which is a down-propagating term, and a scattered-transmitted field, which is up-propagating. Such fields are expressed through cylindrical waves as basis functions, which, in turn, are expressed through plane-wave spectra, and the reflection and transmission coefficients relevant to a plane wave imping on a multilayered medium are included in these spectra. The numerical implementation turns out to be extremely fast, also when modeling very large domains, especially if compared to full-wave techniques involving a discretization of the simulation domain, as with the FDTD. In the numerical results, it is shown the flexibility of the layout in the modeling applications. In particular, the multilayered medium placed above the targets may represent a stratified soil, or the stratification of a road, with different asphalt layers and cement basement. Otherwise, interesting applications are in the modeling of Through-the-Wall radar, from the point of view, for example, of the wall itself, which may be the results of different construction materials. A further possibility is in the modeling of deeply hidden target in a buildings' interior. As shown, the proposed layout can be implemented to model two walls embedding a room, and hiding the targets behind. The paper is organized as follows: in Section II, the developed theory for the CWA is presented; in Section III, numerical results are reported, finally conclusions are drawn in Section IV.

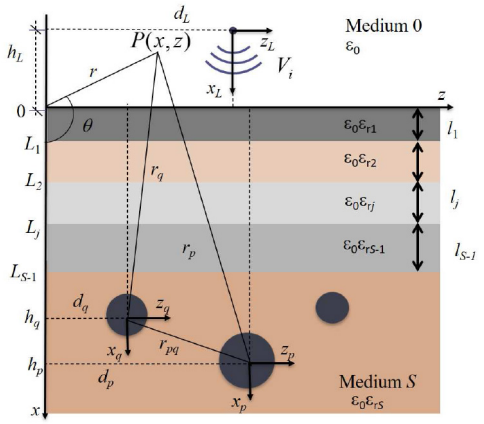

FIGURE 1. Geometry of the scattering problem.

II. THEORETICAL ANALYSIS

The geometry of the problem is shown in Fig. 1. A multilayered medium between two dielectric half-spaces is considered, i.e., medium 0, and medium S. Medium 0 is filled by the vacuum permittivity ε_0, whereas the other media have permittivity $\varepsilon_j = \varepsilon_0\varepsilon_{rj}$ $(j = 1, \ldots, S)$, with $n_j = \sqrt{\varepsilon_{rj}}$ the refraction index of the j-th medium, and they are linear, isotropic, homogeneous, dielectric and lossless. The depth along the x-direction of the j-th layer is in $x = L_j$, with $(j = 1, \ldots, S-1)$, being the first interface in the $x = 0$ axis. The thickness of the j-th layer is $l_j = L_j - L_{j-1}$, with $L_0 = 0$, and $x = L_{j-1}$ and $x = L_j$ denoting the coordinates that bound the layer. N perfectly conducting and circular cross-section cylinders are buried in medium S. The overall problem is two-dimensional, as the cylinders have parallel axes, which are parallel to the flat interfaces too, and they infinitely extend along the y-direction. Cylinders have radii a_q, and axis centred in (h_q, d_q), with $(q = 1, \ldots, N)$, in the main reference frame MRF (O, x, z). A set of reference frames RF_q centred on the q-th $(q = 1, \ldots, N)$ cylinder is also used, in rectangular (O_q, x_q, z_q) or polar (O_q, r_q, θ_q) coordinates, where $x_q = x - h_q$, $z_q = z - d_q$.

As source of the scattering problem a line source in medium 0 is considered, centered in the origin of the reference frame (O_L, x_L, z_L), with $x_L = x - h_L$, $z_L = z - d_L$, being $(h_L < 0, d_L)$, where d_L can be either > 0 or < 0, its center position in MRF. The problem is solved for a monochromatic source of frequency f, and the term $exp(-j\omega t)$, with $\omega = 2\pi f$ the angular frequency, will be omitted in the analysis.

All the geometrical lengths are normalized to the vacuum wavenumber $k_0 = 2\pi f/c$, being c the vacuum speed of light. As to the main reference frame *(MRF)*, the normalized coordinates (O, ξ, ζ) are employed, obtained as follows

$$\begin{aligned} \xi &= k_0 x \\ \zeta &= k_0 z \end{aligned} \tag{1}$$

In the normalized analysis, the other geometrical parameters are $\alpha_q = k_0 a_q$, $(\chi_q = k_0 h_q$, $\eta_q = k_0 d_q)$, with $(q = 1, \ldots, N)$, in MRF. As to the references frames RF_q, it is (O_q, ξ_q, ζ_q),

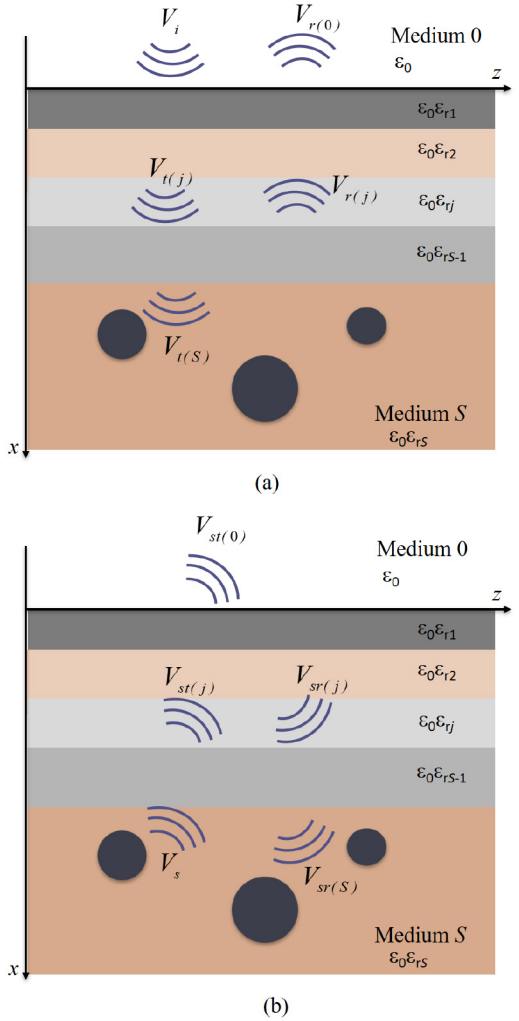

FIGURE 2. Decomposition of the total field: a) source fields; b) scattered fields.

with $\xi_q = k_0 x_q$, $\zeta_q = k_0 z_q$, and (O_q, ρ_q, θ_q), with $\rho_q = k_0 r_q$. In a similar manner, for the source, it is (O_q, ξ_L, ζ_L), with $\eta_L = k_0 h_L$, $\chi_L = k_0 d_L$. Normalized depth of the j-th interface is given by $\Lambda_j = k_0 L_j$.

The scattering problem is solved in terms of the function $V(\xi, \zeta)$, which stands for the y-directed electric field $E_y(\xi, \zeta)$ in the $TM^{(y)}$ polarization state, and for the y-directed magnetic field $H_y(x, z; t)$ in the $TE^{(y)}$ one.

As shown in Fig. 2, two classes of fields are excited. In Fig. 2(a), a first group is given by the incident line source, and the relevant transmitted and reflected contributions by the interfaces of the multilayer medium (Fig. 2(a)), i.e., they are fields that propagate also in the absence of the cylinders. They form two sets of waves, a down-propagating one, given by the transmitted fields from the line-source excitation, and an up-propagating wave relevant to the reflected fields, denoted as follows:

- $V_i(\xi, \zeta)$: line-source incident field;
- $V_r(j)(\xi, \zeta)$: line-source reflected field in medium j ($j = 1, \ldots, S-1$), due to the reflection of the incident line source V_i by the interfaces;
- $V_{t(j)}(\xi, \zeta)$: line-source transmitted field in medium j ($j = 1, \ldots, S$), due to the transmission of the incident line-source V_i through the interfaces;

A second group of fields is given by the scattered fields (Fig. 2(b)):

- $V_s(\xi, \zeta)$: field scattered by the cylinders in medium S;
- $V_{sr(j)}(\xi, \zeta)$: scattered-reflected field in medium j ($j = 1, \ldots, S$), due to reflection of V_s by the $(j-1)$-th interface;
- $V_{st(j)}(\xi, \zeta)$: scattered-transmitted field in medium j ($j = 0, \ldots, S-1$), due to the transmission of V_s through the j-th interface.

Let us consider the expression of the field radiated by the line source, in the normalized coordinates of MRF:

$$V_i(\xi, \zeta) = -V_0 H_0^{(1)}\left[n_0\sqrt{(\xi - \chi_L)^2 + (\zeta - \eta_L)^2}\right] \quad (2)$$

where V_0 is the complex amplitude of the incident field, and $H_0^{(1)}$ is the first-kind Hankel function of zero-th order.

An alternative expression of $H_0^{(1)}$ is as a zero-th order cylindrical wave CW_0, expressed through a plane-wave spectrum

$$CW_0(\xi, \zeta) = \frac{1}{2\pi}\int_{-\infty}^{+\infty} F_0(\xi, n_\parallel) e^{in_\parallel \zeta} dn_\parallel \quad (3)$$

where $n_\parallel$ is the parallel component of the normalized wavevector $\mathbf{k}/k_0 = \mathbf{n} = n_\perp \hat{\mathrm{x}} + n_\parallel \hat{\mathrm{z}}$, and $n_\perp = \sqrt{1 - (n_\parallel)^2}$ the orthogonal component, and being for the spectrum F_0

$$F_0(\xi, n_\parallel) = \frac{2}{\sqrt{1 - n_\parallel^2}} e^{i\xi\sqrt{1-n_\parallel^2}} \quad (4)$$

The representation (3) allows to derive the zero-th order cylindrical waves reflected and transmitted through the interfaces, as the incident field V_i impinges on the multilayer. In particular, the field transmitted in medium S, where the cylinders are buried, can be expressed as:

$$V_{t(S)}(\xi, \zeta) = -V_0 CW_{0t}^{(S)}(\xi - \Lambda_{S-1}, \zeta - \eta_L, -\chi_L) \quad (5)$$

with $CW_{0t}^{(S)}$ the zero-th order transmitted cylindrical wave in medium S

$$CW_{0t}^{(S)}(\xi, \zeta, -\chi_L) = \frac{1}{2\pi}\int_{-\infty}^{+\infty} T_{0,S} F_0(-\chi_L, n_\parallel) \times e^{in_S\sqrt{1-(n_\parallel/n_S)^2}(\xi - \Lambda_{S-1})} \times e^{in_\parallel(\zeta - \eta_L)} dn_\parallel \quad (6)$$

In (6), $T_{0,S}$ is the transmission coefficient from medium 0 to medium S. Its expression is the one relevant to a multilayer

medium [40], and takes into account all the multiple reflections inside the slabs. The expression (5) is also written in polar coordinates, in order to make easier the imposition of the boundary conditions on the cylinders' interfaces, as it will be shown in the following:

$$V_{\mathrm{t}(S)}(\xi,\zeta) = -V_0 \sum_{\ell=-\infty}^{\infty} J_\ell(n_S\rho_\mathrm{p}) e^{i\ell\theta_\mathrm{p}} \times CW^{(S)}_{0\ell\mathrm{t}}\big(\chi_\mathrm{p} - \Lambda_{S-1}, \eta_\mathrm{p} - \eta_L, -\chi_L\big) \quad (7)$$

The (7) is obtained by applying the expansion of a plane wave into Bessel functions, and as to $CW^{(S)}_{0\ell\mathrm{t}}$ it is:

$$CW^{(S)}_{0\ell\mathrm{t}}(\xi,\zeta,-\chi_L) = \frac{1}{2\pi}\int_{-\infty}^{+\infty} T_{0,S} F_0\big(-\chi_L, n_\parallel\big) \times e^{in_S\sqrt{1-(n_\parallel/n_S)^2}(\chi_\mathrm{p}-\Lambda_{S-1})} e^{i n_\parallel} \times \big(\eta_\mathrm{p} - \eta_L\big) e^{-i\ell\frac{n_\parallel}{n_\perp}} dn_\parallel \quad (8)$$

Due to propagation of the field (5) in medium S, the scattered field V_s is excited by the cylinder. It is the sum of the fields scattered by each cylinder, which, in turn, are superpositions of cylindrical functions through unknown expansion coefficients c_qm, in the following way [21]:

$$V_\mathrm{s}(\xi,\zeta) = \sum_{\mathrm{q}=1}^{N}\sum_{m=-\infty}^{+\infty} c_\mathrm{qm} CW_\mathrm{m}\big(n_S\xi_\mathrm{q}, n_S\zeta_\mathrm{q}\big) \quad (9)$$

where

$$CW_\mathrm{m}\big(n_S\xi_\mathrm{p}, n_S\zeta_\mathrm{p}\big) = H^{(1)}_\mathrm{m}\big(n_S\rho_\mathrm{p}\big) e^{i\mathrm{m}\theta_\mathrm{p}} \quad (10)$$

being $H^{(1)}_\mathrm{m}$ the first-kind Hankel function of integer order m.

The incidence of the scattered field V_s on the interfaces of the multilayer above gives rise to two sets of scattered fields, down-propagating scattered-reflected fields, and up-propagating scattered-transmitted fields. In order to derive such contributions, the cylindrical functions CW_m in (9) are expressed making use again of the concept of plane-wave spectrum of a cylindrical wave [41]

$$CW_\mathrm{m}(\xi,\zeta) = \frac{1}{2\pi}\int_{-\infty}^{+\infty} F_\mathrm{m}\big(\xi, n_\parallel\big) e^{i n_\parallel \zeta} dn_\parallel \quad (11)$$

The (11) generalizes the expression (3), being as to the plane-wave spectrum F_m:

$$F_\mathrm{m}\big(\xi, n_\parallel\big) = \frac{2}{\sqrt{1-n_\parallel^2}} e^{i|\xi|\sqrt{1-n_\parallel^2}} \begin{cases} e^{i\mathrm{m}\arccos n_\parallel}, & \xi \geq 0 \\ e^{-i\mathrm{m}\arccos n_\parallel}, & \xi \leq 0 \end{cases} \quad (12)$$

where in (11) and (12) $n_\parallel$ is the parallel component of the normalized wavevector $\mathbf{k}/k_0 = \mathbf{n} = n_\perp\hat{\mathrm{x}} + n_\parallel\hat{\mathrm{z}}$, with $n_\perp = \sqrt{1-(n_\parallel)^2}$.

Transmitted cylindrical waves of order m for the j-th medium, $TW^{(j)}_\mathrm{m}$ $(j = 0,\ldots,S-1)$, are obtained from the spectral cylindrical functions (11). The propagation term is defined through a normalized reflected wavevector $n^{\mathrm{t}(j)} = -\sqrt{1-(n_S n_\parallel/n_j)^2}\hat{\mathbf{x}} + (n_S n_\parallel/n_j)\hat{\mathrm{z}}$, whereas the amplitude is given by the coefficient $T_{S,j}(n_\parallel)$ [40], i.e., the transmission coefficient from medium S to medium j (see the Appendix for the derivation of this coefficient and coefficients employed in the following expressions):

$$TW^{(j)}_\mathrm{m}(u,v,w) = \frac{1}{2\pi}\int_{-\infty}^{\infty} T_{S,j}\big(n_\parallel\big) \times F_\mathrm{m}\big(w, n_\parallel\big) e^{-in_j\sqrt{1-(n_S n_\parallel/n_j)^2}u} e^{in_S n_\parallel v} dn_\parallel \quad (13)$$

The (13) are used as basis functions for the scattered-transmitted field $V_{\mathrm{st}}(j)$:

$$V_{\mathrm{st}(j)}(\xi,\zeta) = \sum_{\mathrm{q}=1}^{\mathrm{N}}\sum_{\mathrm{m}=-\infty}^{\infty} i^\mathrm{m} c_\mathrm{qm} \times TW^{(j)}_\mathrm{m}\big[\xi - \Lambda_j, \zeta - \eta_\mathrm{q}, -n_S\big(\chi_\mathrm{p} - \Lambda_{S-1}\big)\big] \quad (14)$$

In a similar manner, reflected cylindrical waves of order m in the j-th medium, $RW^{(j)}_\mathrm{m}$ $(j = 1,\ldots,M)$, are obtained: the propagation term is defined through a normalized reflected wavevector $n^{\mathrm{r}(j)} = -n_\perp\hat{\mathrm{x}} + n_\parallel\hat{\mathrm{z}}$, whereas the amplitude is given by the coefficient $T_{S,j}(n_\parallel)\Gamma_{j,j-1}(n_\parallel)$, where $\Gamma_{j,j-1}(n_\parallel)$ the reflection coefficient at the interface between medium $j-1$ and medium j (see the Appendix for their derivation):

$$RW^{(j)}_\mathrm{m}(u,v,w) = \frac{1}{2\pi}\int_{-\infty}^{\infty} T_{S,j}\big(n_\parallel\big)\Gamma_{j,j-1}\big(n_\parallel\big) \times F_\mathrm{m}\big(w, n_\parallel\big) e^{i\sqrt{1-(n_\parallel)^2}u} e^{in_\parallel v} dn_\parallel \quad (15)$$

The (15) can be rewritten in the following more compact form, which takes into account the definition of the spectrum (12)

$$RW^{(j)}_\mathrm{m}(u+w,v) = \frac{1}{2\pi}\int_{-\infty}^{\infty} T_{S,j}\big(n_\parallel\big)\Gamma_{j,j-1}\big(n_\parallel\big) \times F_\mathrm{m}\big(w+u, n_\parallel\big) e^{in_\parallel v} dn_\parallel \quad (16)$$

The (16) are used as basis functions for the scattered-reflected field $V_{\mathrm{st}(j)}$:

$$V_{\mathrm{sr}(j)}(\xi,\zeta) = \sum_{\mathrm{q}=1}^{\mathrm{N}}\sum_{\mathrm{m}=-\infty}^{\infty} c_\mathrm{qm}\frac{1}{2\pi}\int_{-\infty}^{\infty} T_{S,j}\big(n_\parallel\big)\Gamma_{j,j-1}\big(n_\parallel\big) \times F_\mathrm{m}\big[-n_S\big(\xi - \Lambda_{j-1} + \chi_\mathrm{p} - \Lambda_{S-1}\big), n_\parallel\big] \times e^{in_S n_\parallel(\zeta-\eta_\mathrm{p})} dn_\parallel \quad (17)$$

The final solution of the scattering problem is found imposing boundary's conditions on the interface of the cylinders. For this task, the fields propagating in the lowest medium, hosting the cylindrical targets, are expressed in polar coordinates, centered on the cylinders' axis. As to the scattered field (9), its expression in polar coordinates of RF_p is obtained making use of the addition theorem of Hankel

functions [44]:

$$V_s(\xi,\zeta) = \sum_{\ell=-\infty}^{\infty} J_\ell(n_S\rho_p)e^{i\ell\theta_p} \times \sum_{q=1}^{N}\sum_{m=-\infty}^{\infty} c_{qm}\left[CW_{m-\ell}(n_S\xi_{qp}, n_S\zeta_{qp}) \times (1-\delta_{qp}) + \frac{H_\ell^{(1)}(n_S\rho_q)}{J_\ell(n_S\rho_q)}\delta_{qp}\delta_{\ell m}\right] \quad (18)$$

where δ is the Kronecker symbol.

The scattered reflected field $V_{sr(S)}$ in medium S, evaluated for $j = S$ from the general expression (17), is expressed as a function of the coordinates in RF_p, by means of the expansion of a plane-wave into Bessel functions

$$V_{sr(S)}(\xi,\zeta) = \sum_{\ell=-\infty}^{\infty} J_\ell(n_S\rho_p)e^{i\ell\theta_p} \times \sum_{q=1}^{N}\sum_{m=-\infty}^{\infty} c_{qm}\frac{1}{2\pi}\int_{-\infty}^{\infty}\Gamma_{S,S-1}(n_\parallel) \times F_m\left[-n_S(\chi_p+\chi_q-2\Lambda_{S-1}), n_\parallel\right] \times e^{in_\parallel n_S(\eta_p-\eta_q)}dn_\parallel \quad (19)$$

By imposing the boundary conditions on the surface of each cylinder, in TM polarization we have

$$\left[V_{t(S)}+V_s+V_{sr(S)}\right]_{\rho_p=\alpha_p} = 0 \quad p = 1,\ldots,N \quad (20)$$

while in TE polarization:

$$\frac{\partial}{\partial\rho_p}\left[V_{t(S)}+V_s+V_{sr(S)}\right]_{\rho_p=\alpha_p} = 0, \quad p = 1,\ldots,N \quad (21)$$

By introducing the (7), (18), and (19) in (20) and (21), after some manipulations the following linear system is obtained

$$\sum_{q=1}^{N}\sum_{m=-\infty}^{\infty} A_{\ell m}^{qp\,(TM,\,TE)}c_{qm} = B_\ell^{p\,(TM,\,TE)} \quad p = 1,\ldots,N \quad \ell = -\infty,\ldots,\infty \quad (22)$$

with

$$A_{\ell m}^{qp(TM,TE)} = i^{m-\ell}e^{-im}\left\{CW_{m-\ell}(n_S\xi_{qp}, n_S\zeta_{qp})(1-\delta_{qp}) + RW_{m+\ell}^{(j)}\left[-n_S(\chi_q+\chi_p-2\Lambda_{S-1}), n_S(\eta_p-\eta_q)\right] + \frac{\delta_{m\ell}\delta_{qp}}{G_\ell^{(TM,TE)}(n_S\alpha_p)}\right\} \quad (23)$$

$$B_\ell^{p(TM,TE)} = -G_\ell^{(TM,TE)}(n_S\alpha_p)V_0 \times CW_{0\ell t}^{(S)}(\chi_p-\Lambda_{S-1}, \eta_p-\eta_L, -\chi_L) \quad (24)$$

with $G_\ell^{(TM)}(\cdot) \equiv J_\ell(\cdot)/H_\ell^{(1)}$, and $G_\ell^{(TE)}(\cdot) \equiv J'_\ell(\cdot)/H'^{(1)}_\ell$, and the prime denoting derivation. Once the expansion coefficients c_{qm} have been found, the scattered fields are determined for each frequency f of the spectrum.

III. NUMERICAL RESULTS

The theory described in Section II has been implemented in a numerical code. The numerical evaluation of the spectral integrals relevant to the cylindrical functions RW_m, TW_m is performed according to the algorithm developed in [42] and [43], respectively. The infinite series relevant to the expansion into cylindrical waves are truncated applying the rule $M = \lfloor 3n_{j\mathrm{MAX}}\alpha_{p\mathrm{MAX}}\rfloor$ [45], where $n_{j\mathrm{MAX}}$ is the highest refraction index among n_j, with $j = 1,\ldots,S$, and $\alpha_{p\mathrm{MAX}}$ the largest cylinder among α_p, with $p = 1,\ldots,N$. This rule allows a good compromise between accuracy and computational heaviness.

As polarization of the incident field, the TM state is considered in the numerical results presented in this Section, corresponding to a line source aligned parallel to the cylinders' axis. The method is preliminary validated, through comparisons with gprMax [24], a software developed with the FDTD technique. The inverse FFT is applied to the numerical solution by gprMax, to return the scattered field at the wanted frequency, in order to compare its results with the CWA presented in Section II. The case of validation is performed considering a layout with applications to GPR surveys of targets buried in the subsoil. The multilayered medium is a possible background in the subsurface analysis, made by different layers of soils and rocks. In the example shown in Fig. 3(a), the multilayer is modeling a road pavement above a semi-infinite soil. In particular, an asphalt layer of thickness $l_1 = 0.05$ m and relative permittivity $\varepsilon_{r1} = 7$ (medium 1), is followed by an asphalt base with $l_2 = 0.15$ m and $\varepsilon_{r2} = 5$ (medium 2), and by a concrete basement with $l_3 = 0.25$ m and $\varepsilon_{r3} = 10$ (medium 3). The final semi-infinite medium (medium 4) is a soil of relative permittivity $\varepsilon_{r4} = 4$, where a metallic rebar, of radius $a = 0.05$ m, is buried in ($d_1 = 0.95$ m,$h_1 = 0$ m) in MRF. The line source, of frequency $f = 600$ MHz, is placed in ($d_L = -0.3$ m, $h_L = 0$ m), and has a unit amplitude $V_0 = 1$ V/m. The scattered field is probed in 41 points along a line parallel to the interface in medium 0, in $x = -0.3$ m. Comparison between CWA and gprMax in Fig. 3(b) shows a very good agreement. In the presented layout, the number of terms employed in the simulations with CWA, by application of the rule $M = \lfloor 3n_{j\mathrm{MAX}}\alpha_{p\mathrm{MAX}}\rfloor$, is $M = 6$, obtained from the highest refraction index $n_3 = \sqrt{10}$ and the cylinder radius $a_1 = 0.05$ m, normalized at 600 MHz. The different values of the truncation index M are also shown in Table 1, for smaller and larger values of the cylinder radius, in the same background of Fig. 3. In the same table, computational times of the CWA simulations evaluated an Intel CORE i7 CPU

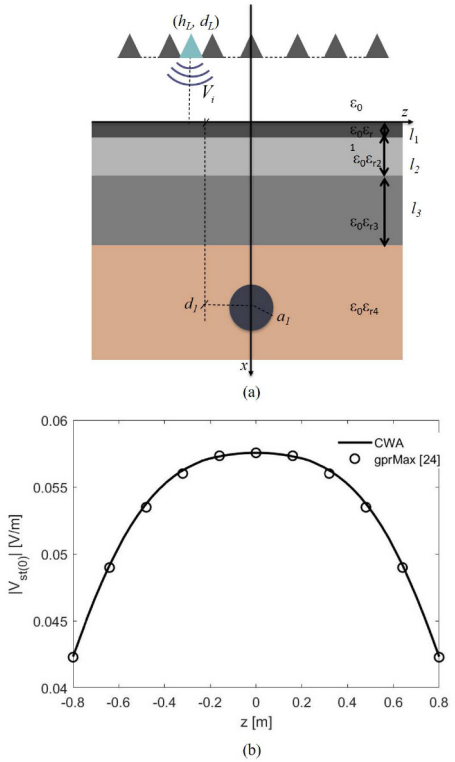

FIGURE 3. a) Geometry of a geophysical layout with $M = 4$ media; (b) Scattered-transmitted field in medium 0 probed in $x = -0.3$ m for a line source of amplitude $V_0 = 1$ V/m placed in $(-0.3$ m, 0), with $l_1 = 0.05$ m, $\varepsilon_{r1} = 7$; $l_2 = 0.15$ m, $\varepsilon_{r2} = 5$; $l_3 = 0.25$ m, $\varepsilon_{r3} = 10$; $\varepsilon_{r4} = 4$, and one perfectly conducting rebar of radius $a = 0.05$ m and centre in $(d_1 = 0.95$ m,$h_1 = 0$ m).

TABLE 1. Comparison between the execution times for Gprmax [24] and the CWA for the layout of Fig. 3. The number of receivers is $N = 41$.

	CWA		Gprmax
radius [m]	M	execution time [sec]	execution time [sec]
a=0.05	6	1.4	1644.1
a=0.01	11	2.6	1700.4
a=0.25	29	7.8	1694.9

@2.70 GHz, RAM 8 GB, are also reported, and compared to the ones of gprMax, run for a time window of 60 ns and a layout of size (2.4 m × 2.2 m × 0.005 m), to achieve convergence of the frequency-domain results. The CWA turns out to be extremely fast, and execution times are increased as the cylinder radius is enlarged, as a higher number of terms M is included in the evaluation of the cylindrical functions. Execution times are instead almost comparable and independent on the target size, but determined by overall size of the domain, of the elementary cell, and length of the time window.

In the second example of application, a three-layer layout as the one depicted in Fig. 3 is considered. In the choice of the physical parameters of the multilayer, the possibility of modeling a void layer as an anomaly in the road basement above the cylinder is included. Medium 1 is an asphalt layer of thickness $l_1 = 0.10$ m and relative permittivity $\varepsilon_{r1} = 5$, followed by a thin void layer of thickness $l_2 = 0.03$ m and

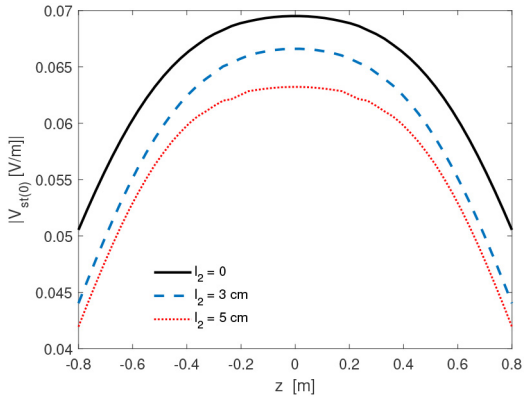

FIGURE 4. Scattered-transmitted field in medium 0 in $x = -0.3$ m for a line source in $(d_L = -0.3$ m, $h_L = 0$ m) at 600 MHz and one cylinder of radius $a_1 = 0.05$ m in $(d_1 = L_3 + 0.5$ m, $h_1 = 0$ m). $S = 4$ media with $\varepsilon_{r1} = 5$, $l_1 = 0.10$ m, $\varepsilon_{r3} = 10$, $l_3 = 0.25$, $\varepsilon_{r4} = 4$, and as to medium 2, $\varepsilon_{r2} = 1$, and different thicknesses l_2 are compared.

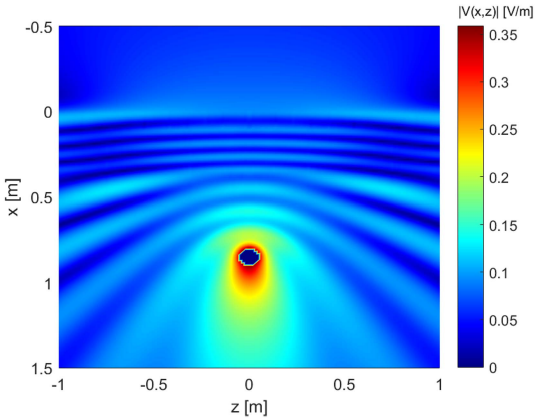

FIGURE 5. Two-dimensional field map of the total scattered electric field for the same layout of Fig. 4, when $l_2 = 0$.

vacuum-like permittivity $\varepsilon_{r2} = 1$ (medium 2), a concrete basement with $l_3 = 0.25$ m and $\varepsilon_{r3} = 10$ (medium 3), and finally by a soil with $\varepsilon_{r4} = 4$ (medium 4). A metallic rebar of radius $a = 0.05$ m is buried in medium 4, with centre in $(d_1 = L_3 + 0.5$ m, $h_1 = 0$ m) in MRF, being $L_3 = l_1 + l_2 + l_3$. The line source is placed in $(d_L = -0.3$ m, $h_L = 0$ m), has frequency $f = 600$ MHz, and amplitude $V_0 = 1$ V/m. The results of the scattered-transmitted field in medium 0, along a line parallel to the interface in $x = -0.3$ m, are reported in Fig. 4, and compared to the case of a thicker void layer $l_2 = 0.05$ m, and absence of the void, with $l_2 = 0$, showing the sensitivity of the scattered field to the properties of the background. The total scattered field in air, in the multilayer, and in the final semi-infinite medium is reported in the two-dimensional field map in Fig. 5 in the case $l_2 = 0$.

The layout of the scattering problem presented in Section II has also interesting applications in the radar surveys of targets placed behind a wall, with the Through-the-Wall radar. The multilayered medium may deal with stratified walls, where the masonry is the results of different

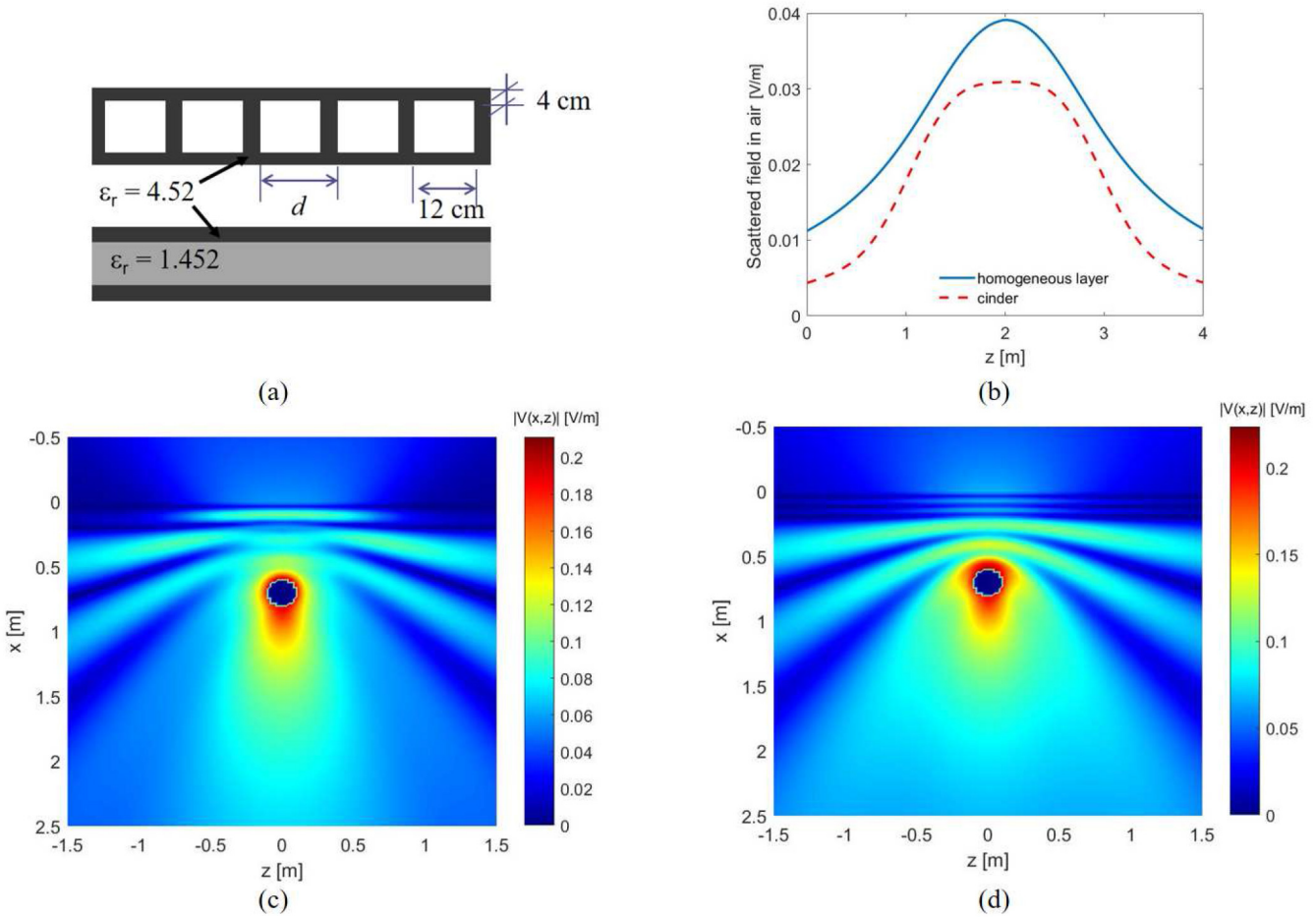

FIGURE 6. a) Geometry of cinder-wall layout, having periodic square blocks, and homogenized model of cinder according to [4], where the periodic internal layout is replaced by a homogeneous slab of equivalent permittivity $\varepsilon_2 = 1.452$. Results relevant to one cylinder of radius $a = 0.09$ m and center in ($d_1 = 1.2$ m, $h_1 = 0$ m) below a cinder-block wall given by the equivalent three layer model ($l_1 = l_3 = 4$ cm, $\varepsilon_{r1} = \varepsilon_{r3} = 4.52$, $l_2 = 12$ cm, $\varepsilon_{r2} = 1.452$) at 600 MHz: b) scattered-transmitted field in $x = -0.1$ m (solid line), compared to the modeling of the wall as a single layer with $l_1 = 20$ cm, $\varepsilon_{r1} = 4.52$ (dotted line); c) two-dimensional field map of the total scattered field; d) two-dimensional field map of the total scattered field, when the wall is a single layer with $l_1 = 20$ cm, $\varepsilon_{r1} = 4.52$.

layers of construction materials, or may models panels like plywoods assembled to make internal partitions of the wall.

An common example of wall is given by cinder-block wall, that is non-homogeneous. It has periodic layout of square air-holes in a concrete layer, as depicted in Fig. 6(a), which, however, may modeled with three homogeneous layers in the x-direction, applying the equivalent model described in [4], shown in the same picture, obtained from homogenization of the internal structure. Total thickness of cinder-block wall, as presented in [4], is 20 cm, and in the equivalent model it is replaced by two external layers of thickness $l_1 = l_3 = 4$ cm and permittivity $\varepsilon_{r1} = \varepsilon_{r3} = 4.52$, and an intermediate and homogeneous layer of thickness $l_2 = 12$ cm and equivalent permittivity $\varepsilon_{r2} = 1.452$. This stratified layout can be applied to the analysis of a layered background with CWA. In the final medium, a perfectly conducting target of radius $a_1 = 9$ cm is placed with center in ($h_1 = 1.2$ m, $d_1 = 0$). The line source is in ($d_L = -0.1$ m, $h_L = 0$ m), and $V_0 = 1$ V/m. Results in Fig. 6(b) are relevant to the scattered-transmitted field in medium 0, evaluated along a line in $x = -0.1$ m, and compared to the case of modeling one layer of identical overall thickness $l_1 = 20$ cm and relative permittivity $\varepsilon_{r1} = 4.52$. Results show the different focusing effect introduced by the single layer and the three-layer modeling of the wall on the scattered field by the cylinder.

Results of the two-dimensional field map of the total scattered field by the cylinder at the frequency of 1 GHz are reported in Fig. 6(c) and 6(d): Fig. 6(c) is relevant the equivalent three-layer model of cinder-block, whereas in Fig. 6(d) the wall is one homogeneous layer, as already considered in Fig. 6(b). Size of the target is compatible with a human head, and its physical modeling as a perfect-electric conducting medium can well approximate the high reflectivity of biological tissues at 1 GHz.

Another interesting application of the method with the Through-the-Wall radar is the search of targets that, in a buildings' interior, are hidden behind a room, as described in the picture of Fig. 7(a). In particular, the layout above the target is made by external two walls, whereas the internal space is a vacuum-filled medium ($\varepsilon_{r3} = 1$) with length $l_2 =$

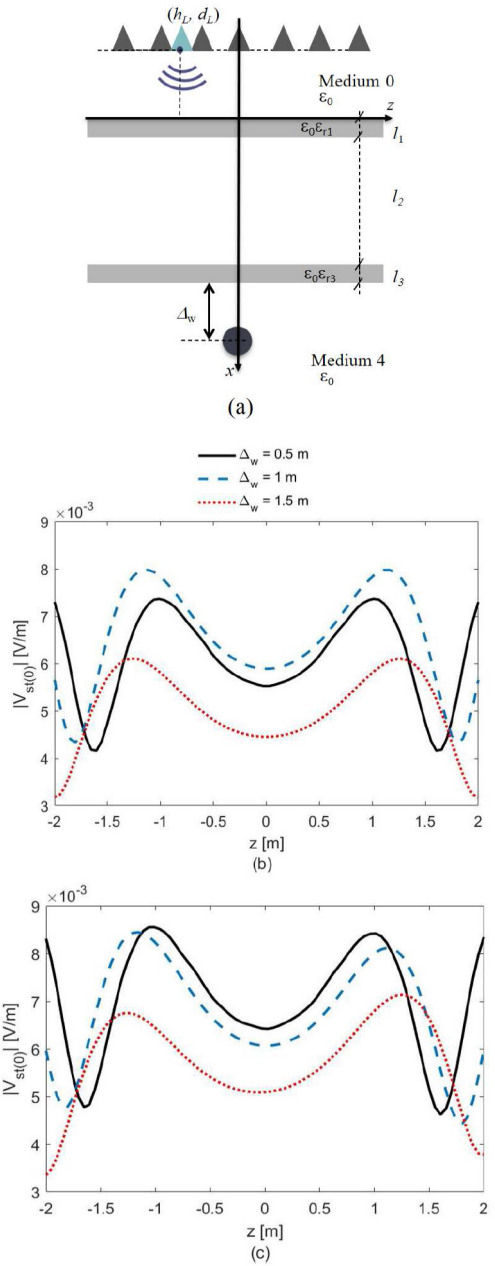

FIGURE 7. a) Geometrical layout; Scattered-transmitted field in medium 0 by one cylinder of radius $a_1 = 0.1$ m for a line source at 1 GHz and with centre in $((h_L = -0.3$ m, $d_L)$, with: b) $d_L = 0$; c) $d_L = -1$ m.

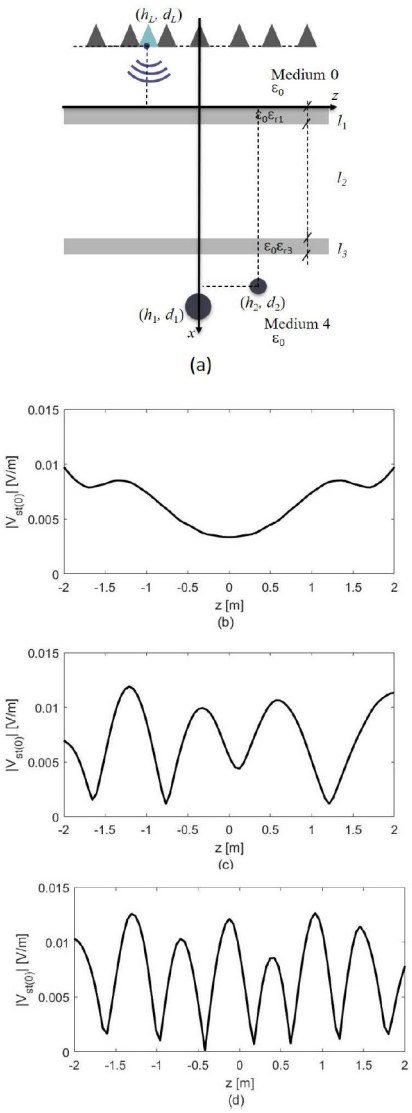

FIGURE 8. a) Geometrical layout. Scattered-transmitted field in medium 0 by two cylinders, with cylinder 1 in ($h_1 = 4.9$ m, $d_1 = 0$) and cylinder 2 ($h_2 = 3.9$ m, d_2) with: b) $d_2 = 0$; c)$d_2 = 0.5$ m; d) $d_2 = 1.5$ m.

2 m. The two walls have thickness $l_1 = l_3 = 0.2$ m and relative permittivities $\varepsilon_{r1} = \varepsilon_{r3} = 6$. Results are evaluated for a target with radius $a_1 = 0.1$ m, with centre in $(d_1, 0)$ in the final medium (medium 4, $\varepsilon_{r4} = 1$), at different depths d_1 of the cylinder. In particular, distance between cylinder center and the second wall is described by the parameter Δ_w, with $\Delta_w = 0.5$ m, 1 m, and 1.5 m. The line source has centre along the x-axis in $h_L = -0.3$ m; horizontal position is aligned with the centre of the target, with $d_L = 0$ in Fig. 7(a), and placed at a lateral distance $d_L = -1$ m in Fig. 7(b). Frequency of the source is $f = 1$ GHz, and amplitude $V_0 = 1$ V/m. Two cylinders are considered in the layout of Fig. 8(a): cylinder 1 has radius $a_1 = 0.1$ m, with centre in ($h_1 = 4.9$ m, $d_1 = 0$), and cylinder 2 has radius $a_2 = 0.05$ m, centre in ($h_2 = 3.9$ m, d_2), and three values of the horizontal distance d_2 are considered: $d_2 = 0$ (cylinder 2 is placed above cylinder 1), and $d_2 = 0.5$, 1.5 m. The source is the same of the one in Fig. 7, and centred in ($h_L = -0.3$ m, $d_L = 0$). The effects of mutual interaction between the two targats can be appreciated in these plots. Execution times relevant to the cases of Fig. 8 are reported in Table 2, and they can be considered very low with reference to the size of the simulation domain, which is mainly determined by the depth and lateral distance of the cylinders.

IV. CONCLUSION

In this article, a technique to solve the scattering of the field radiated by a line source from cylinders placed below

TABLE 2. Execution times for the layout of Fig. 8. The number of receivers is $N = 41$.

	Fig. 8(b)	Fig. 8(c)	Fig. 8(d)
Execution time [sec]	28	28.9	29.3

a multilayer has been presented. The approach has been developed in the frequency domain, through the CWA, evaluating the scattered fields with a semi-analytical formulation. Advantages of the technique are in the fast computational times, also for very large domains, and accuracy of the results. It has been shown that the layout has applications in several fields. The multilayer can model a stratified ground, to evaluate the scattered field by a target in GPR surveys. Otherwise, applications can be in the Through-the-Wall radar modeling, when targets are placed below a stratified wall, or hidden behind multiple walls in an internal room. Another interesting application of the approach may be in the modeling of biological tissues, where the buried scatters may represent an implanted antenna. The different tissues, as skin, muscle, fat or bones, would be included in the stratified background model. However, this extension should model the significant losses in the dielectric permittivity that are typical of biological media at microwave frequencies, which have been not considered in this article, but will regard future work.

APPENDIX

Here, the derivation of the reflection and transmission coefficients used in the spectral integrals (13) and (16), introduced in the theoretical approach in Section II, is shown. The coefficients are relevant to the interaction with a dielectric multilayer with $S-1$ slabs, $S+1$ dielectric media, and S interfaces (Fig. 1). The recalled integrals are employed in the calculation of the scattered-reflected and scattered-transmitted fields, that are excitated by incidence of the scattered field V_s in medium S on the interface in $\xi = \Lambda_{S-1}$ and propagating up to medium 0 (Fig. 3). According to this layout, the incident and reflected fields are considered at the right of each interface in $\xi = \Lambda_j$ $(j = S-1, ..., 0)$.

Let us define as E_j^+ the amplitude of the forward field in the j-th medium (propagating upward from medium S), with $j = 0, \ldots, S$, and E_j^- the amplitude of the backward field (propagating downward from medium 1), with $j = 1, \ldots, S$, as in medium 0 $E_0^- = 0$. The fields $E_j^\pm$ can be considered as the amplitudes of a generic plane wave in the plane-wave spectra (13) and (16), relevant to the scattered fields in Fig. 2(b).

The elementary reflection coefficients ρ_j at the S interfaces are defined in terms of the refractive indices as follows:

$$\rho_j = \frac{\eta_{j+1} - \eta_j}{\eta_{j+1} + \eta_j}, \quad j = S-1, \ldots, 0 \tag{25}$$

whereas the elementary transmission coefficients τ_j at the S interfaces are:

$$\tau_j = \frac{2\eta_{j+1}}{\eta_{j+1} + \eta_j}, \quad j = S-1, \ldots, 0 \tag{26}$$

In (25), (26) the following definitions are employed in each medium:

$$\eta_j = \begin{cases} n_j n_\parallel, & \text{TM polarization} \\ \frac{n_\parallel}{n_j}, & \text{TE polarization} \end{cases}, \quad j = 0, \ldots, S \tag{27}$$

The overall reflection response can be obtained recursively by the propagation of the reflection responses. To obtain the layer recursion, the fields at the left of the interface are related to the one at its right as follows:

$$\begin{bmatrix} E_{j+1}^+ \\ E_{j+1}^- \end{bmatrix} = C_{j+1,j} \begin{bmatrix} E_j^+ \\ E_j^- \end{bmatrix} \quad j = 1, \ldots, S-1 \tag{28}$$

where, in (28), $C_{j+1,j}$ is a matrix that links fields at media j and $j+1$:

$$C_{j+1,j} = \frac{1}{\tau_j} \begin{bmatrix} e^{-i\delta_j} & \rho_j e^{i\delta_j} \\ \rho_j e^{-i\delta_j} & e^{i\delta_j} \end{bmatrix} \quad j = 1, \ldots, S-1 \tag{29}$$

being $\delta_j = \Lambda_j \sqrt{(1 - (n_0 n_\parallel / n_j)^2}$, with $n_0 = 1$, and $e^{\pm i\delta_j}$ gives the propagation term through the j-th layer of normalized thickness Λ_j.

The recursion is initialized starting from the fields at the left of the 0-th interface, that give the fields at the right through:

$$\begin{bmatrix} E_1^+ \\ E_1^- \end{bmatrix} = \frac{1}{\tau_0} \begin{bmatrix} 1 & \rho_0 \\ \rho_0 & 1 \end{bmatrix} \begin{bmatrix} E_0^+ \\ 0 \end{bmatrix} \tag{30}$$

In order to derive the total reflection and transmission coefficients $T_{S,0}$ and $\Gamma_{S,S-1}$, the (28) is applied iteratively from medium 0 to medium S, multiplying all the matrices $C_{j+1,j}$ in (29), and thus obtaining:

$$\begin{bmatrix} E_S^+ \\ E_S^- \end{bmatrix} = C_{1,0} C_{2,1} \cdots C_{S,S-1} \begin{bmatrix} E_0^+ \\ 0 \end{bmatrix} \quad s = 1, \ldots, S-1 \tag{31}$$

which can be rewritten as follows:

$$\begin{bmatrix} E_S^+ \\ E_S^- \end{bmatrix} = \begin{bmatrix} c_{11} & c_{12} \\ c_{21} & c_{22} \end{bmatrix} \begin{bmatrix} E_0^+ \\ 0 \end{bmatrix} \tag{32}$$

having defined a total matrix C of elements c_{11}, c_{12}, c_{21} and c_{22}:

$$C = C_{1,0} C_{2,1} \cdots C_{S,S-1} = \begin{bmatrix} c_{11} & c_{12} \\ c_{21} & c_{22} \end{bmatrix} \tag{33}$$

From the (32), the total transmission coefficient is found as:

$$T_{S,0} = \frac{E_0^+}{E_S^+} = \frac{1}{c_{11}} \tag{34}$$

Similarly, the total reflection coefficient is:

$$\Gamma_{S,S-1} = \frac{E_S^-}{E_S^+} = \frac{c_{21}}{c_{11}} \tag{35}$$

The (34) is employed for the transmitted-cylindrical waves of the scattered-transmitted field (14) in medium 0, and (35)

in the reflected-cylindrical waves of scattered-reflected field (19) in medium S.

The general transmission coefficients relevant to the transmitted-cylindrical wave in the j-th medium are derived through the following definition:

$$T_{S,j}= \frac{E_0^+}{E_S^+}\left(\frac{E_0^+}{E_j^+}\right)^{-1} \tag{36}$$

that is employed in (13), and it is obtained from the (34) and the recursive application of (28) up to medium j. Similarly, the total reflection coefficient used in (16) is:

$$\Gamma_{S,j} = T_{S,j}\left(\frac{E_j^-}{E_j^+}\right) = T_{S,j}\Gamma_{j+1,j} \tag{37}$$

The evaluation of the reflection and transmission coefficients used for the fields in Fig. 2(a), relevant to interaction of the line source with the multilayer, in the absence of the cylinders, as in the expression (8), can be found in an analougous way. The incident and reflected fields mut be considered at the left of each interface, and initializing the recursion from medium S.

REFERENCES

[1] D. J. Daniels, *Surface Penetrating Radar*, 2nd ed. London, U.K.: IEE, 2004.

[2] H. M. Jol, *Ground Penetrating Radar: Theory and Applications*. Amsterdam, The Netherlands: Elsevier Sci. Ltd., 2008.

[3] D. Godman and S. Piro, "GPR remote sensing in archeology," in *Chapter 2 Understanding GPR Via Simulator*. Heidelberg, Germany: Springer-Verlag, 2013.

[4] M. G. Amin, *Through-the-Wall Radar Imaging*. Hoboken, NJ, USA: CRC Press, 2011.

[5] J. E. Peabody, Jr., G. L. Charvat, J. Goodwin, and M. Tobias, "Through-the-wall imaging radar," *Lincoln Lab. J.*, vol. 19, no. 1, pp. 62–72, 2012.

[6] A. Q. Howard, "The electromagnetic fields of a subterranean cylindrical inhomogeneity excited by a line source," *Geophysics*, vol. 37, pp. 975–984, Dec. 1972.

[7] S. O. Ogunade, "Electromagnetic response of an embedded cylinder for line current excitation," *Geophysics*, vol. 46, pp. 45–52, Jan. 1981.

[8] S. F. Mahmoud, S. M. Ali, and J. R. Wait, "Electromagnetic scattering from a buried cylindrical inhomogeneity inside a lossy earth," *Radio Sci.*, vol. 16, no. 6, pp. 1285–1298, Nov./Dec. 1981.

[9] K. Hongo and A. Hamamura, "Asymptotic solutions for the scattered field of plane wave by a cylindrical obstacle buried in a dielectric half-space," *IEEE Trans. Antennas Propag.*, vol. AP-34, no. 11, pp. 1306–1312, Nov. 1986.

[10] M. Di Vico, F. Frezza, L. Pajewski, and G. Schettini, "Scattering by a finite set of perfectly conducting cylinders buried in a dielectric half-space: A spectral-domain solution," *IEEE Trans. Antennas Propag.*, vol. 53, no. 2, pp. 719–727, Feb. 2005.

[11] Y. Altuncu, A. Yapar, and I. Akduman, "On the scattering of electromagnetic waves by bodies buried in a half-space with locally rough interface," *IEEE Trans. Geosci. Remote Sens.*, vol. 44, no. 6, pp. 6573–6592, Jun. 2006.

[12] L. Crocco, M. D'Urso, and T. Isernia, "The contrast source-extended born model for 2D subsurface scattering problems," *Progr. Electr. Res. B*, vol. 17, pp. 343–359, Sep. 2009.

[13] S.-C. Lee, "Scattering by a radially stratified infinite cylinder buried in an absorbing half-space,," *J. Opt. Soc. Amer. A*, vol. 30, no. 4, pp. 565–572, Apr. 2013.

[14] C. Bourlier, N. Pinel, and G. Kubick, *Method of Moments for 2D Scattering Problems. Basic Concepts and Applications*. New York, NY, USA: Wiley, 2013.

[15] M. A. Nasr, I. A. Eshrah, and E. A. Hashish, "Electromagnetic scattering from a buried cylinder using a multiple reflection approach: TM case," *IEEE Trans. Antennas Propag.*, vol. 62, no. 5, pp. 2702–2707, May 2014.

[16] K. A. Michalski and D. Zheng, "Electromagnetic scattering and radiation by surfaces of arbitrary shape in layered media, part I: Theory," *IEEE Trans. Antennas Propag.*, vol. 38, no. 3, pp. 335–344, Mar. 1990.

[17] K. A. Michalski and D. Zheng, "Electromagnetic scattering and radiation by surfaces of arbitrary shape in layered media, part II: Implementation and results for contiguous half-spaces," *IEEE Trans. Antennas Propag.*, vol. 38, no. 3, pp. 345–352, Mar. 1990.

[18] C.-H. Huo and M. Moghaddam, "Electromagnetic scattering from a buried cylinder in layered media with rough interfaces," *IEEE Trans. Antennas Propag.*, vol. 54, no. 8, pp. 2392–2401, Aug. 2006.

[19] C. Li, D. Lesselier, and Y. Zhong, "Full-wave computational model of electromagnetic scattering by arbitrarily rotated 1-D periodic multilayer structure," *IEEE Trans. Antennas Propag.*, vol. 64, no. 3, pp. 1047–1060, Mar. 2016.

[20] F. Frezza, L. Pajewski, C. Ponti, and G. Schettini, "Through-wall electromagnetic scattering by N conducting cylinders," *J. Opt. Soc. Amer.*, vol. 30, no. 8, pp. 1632–1639, Aug. 2013.

[21] C. Ponti and S. Vellucci, "Scattering by conducting cylinders below a dielectric layer with a fast non-iterative approach," *IEEE Trans. Microw. Theory Tech.*, vol. 63, no. 1, pp. 30–39, Jan. 2015.

[22] A. Taflove and S. C. Hagness, *Computational Electrodynamics: The Finite-Difference Time-Domain*. Boston, MA, USA: Artech House, 2000.

[23] C. D. Moss, F. L. Teixeira, Y. E. Yang, and J. A. Kong, "Finite-difference time-domain simulation of scattering from objects in continuous random media," *J. Comput. Phys.*, vol. 313, pp. 532–548, Dec. 2016.

[24] C. Warren, A. Giannopoulos, and I. Giannakis, "gprMax: Open source software to simulate electromagnetic wave propagation for ground penetrating radar," *Comput. Phys. Commun.*, vol. 209, pp. 163–170, Dec. 2016.

[25] F. Soldovieri and R. Solimene, "Through-wall imaging via a linear inverse scattering algorithm," *IEEE Trans. Geosci. Remote Sens. Letters*, vol. 4, no. 4, pp. 513–517, Oct. 2007.

[26] B. Yektakhah and K. Sarabandi, "All-directions through-the-wall radar imaging using a small number of moving transceivers," *IEEE Trans. Geosci. Remote Sens.*, vol. 54, no. 11, pp. 6415–6428, Nov. 2016.

[27] M. Charnley and A. Wood, "Through-the-wall radar detection analysis via numerical modeling of Maxwell's equations," *J. Comput. Phys.*, vol. 313, pp. 532–548, Sep. 2016.

[28] M. Pastorino and A. Randazzo, *Through-the-Wall Imaging Radar*. Boca Raton, FL, USA: Artech House, 2018.

[29] C. Estatico, A. Fedeli, M. Pastorino, and A. Randazzo, "A multifrequency inexact-Newton method in LP banach spaces for buried objects detection," *IEEE Trans. Antennas Propag.*, vol. 63, no. 9, pp. 4198–4204, Sep. 2015.

[30] M. Salucci, G. Oliveri, and A. Massa, "GPR prospecting through an inverse-scattering frequency-hopping multifocusing approach," *IEEE Trans. Geosci. Remote Sens.*, vol. 53, no. 12, pp. 6573–6592, Dec. 2015.

[31] G. Gennarelli, G. Vivone, P. Braca, F. Soldovieri, and M. G. Amin, "Multiple extended target tracking for through-wall radars," *IEEE Trans. Geosci. Remote Sens.*, vol. 53, no. 12, pp. 6482–6494, Dec. 2015.

[32] G. Gennarelli, G. Vivone, P. Braca, F. Soldovieri, and M. G. Amin, "Comparative analysis of two approaches for multipath ghost suppression in radar imaging," *IEEE Trans. Geosci. Remote Sens. Lett.*, vol. 13, no. 9, pp. 1226–1230, Sep. 2016.

[33] C. Estatico, A. Fedeli, M. Pastorino, and A. Randazzo, "Microwave imaging in stratified media: A multifrequency inverse-scattering approach,," in *Proc. 13th Eur. Conf. Antennas Propag. (EuCAP)*, 2019, pp. 305–324.

[34] W. Zhang and A. Hoorfar, "MIMO ground penetrating radar imaging through multilayered subsurface using total variation minimization," *IEEE Trans. Geosci. Remote Sens.*, vol. 57, no. 4, pp. 2107–2115, Apr. 2019.

[35] L.-P. Song and Q. H. Liu, "Ground-penetrating radar landmine imaging: Two-dimensional seismic migration and three-dimensional inverse scattering in layered media," *Radio Sci.*, vol. 40, no. 1, pp. 1–15, Feb. 2005.
[36] W. Zhang, "Two-dimensional microwave tomographic algorithm for radar imaging through multilayered media," *Progr. Electromagn. Res.*, vol. 144, pp. 261–270, Jan. 2014.
[37] M. A. Fiaz, F. Frezza, L. Pajewski, C. Ponti, and G. Schettini, "Scattering by a circular cylinder buried under a slightly rough surface: The cylindrical-wave approach," *IEEE Trans. Antennas Propag.*, vol. 60, no. 2, pp. 2834–2842, Jun. 2012.
[38] M. A. Fiaz, F. Frezza C. Ponti, and G. Schettini, "Electromagnetic scattering by a circular cylinder buried below a slightly rough Gaussian surface," *J. Opt. Soc. Amer. A*, vol. 31, no. 1, pp. 26–34, Jan. 2014.
[39] C. Ponti, M. Santarsiero, and G. Schettini, "Electromagnetic scattering of a pulsed signal by conducting cylindrical targets embedded in a half-space medium," *IEEE Trans. Antennas Propag.*, vol. 65, no. 6, pp. 3073–3083, Jun. 2017.
[40] S. J. Orfanidis, *Electromagnetic Waves and Antennas*, ECE Dept., Rutgers Univ., Brunswick, NJ, USA, 2016
[41] G. Cincotti, F. Gori, M. Santarsiero, F. Frezza, F. Furnò, and G. Schettini, "Plane wave expansion of cylindrical functions," *Opt. Commun.*, vol. 95, pp. 192–198, Jan. 1993.
[42] R. Borghi, F. Frezza, P. Oliverio, M. Santarsiero, and G. Schettini, "Scattering of a generic two-dimensional field by cylindrical structures in the presence of a plane interface," *J. Infrared Mil. Terahertz Waves*, vol. 21, no. 5, pp. 805–827, 2000.
[43] M. Di Vico, F. Frezza, L. Pajewski, and G. Schettini, "Scattering by buried dielectric cylindrical structures," *Radio Sci.*, vol. 40, no. 6, 2005, Art. no. RS6S18.
[44] I. N. Sneddon, *Mixed Boundary Value Problems in Potential Theory.* Amsterdam, The Netherlands: North-Holland, 1966.
[45] A. Z. Elsherbeni, "A comparative study of two-dimensional multiple scattering techniques," *Radio Sci.*, vol. 29, pp. 1023–1033, Jul./Aug. 1994.

CRISTINA PONTI (Member, IEEE) received the Laurea and Laurea Magistralis degrees (*cum laude*) in electronic engineering from the "Sapienza" University of Rome in 2004 and 2006, respectively, and the Ph.D. degree in March 2010. In 2006, she joined the Applied Electronics Department, "Roma Tre" University, Rome, Italy, where from November 2006 to October 2009, she attended the Doctoral School in Biomedical Engineering, Electromagnetism, and Telecommunications. From February to December 2010, she was an Assistant Researcher, and since December 2010 is an Assistant Professor in electromagnetic fields. Her main research interests are in electromagnetic analysis, scattering problems, buried-objects detection, ground penetrating radar, through-the-wall radar, numerical methods, electromagnetics-bandgap materials, antennas, and microwave components for high-power applications. She was a Co-Convener of conference sessions at URSI EMTS 2016, URSI EMTS 2019, and URSI GASS 2021. She is an Associate Editor of *IET Microwaves, Antennas & Propagation*. She is a member of the IEEE Antennas and Propagation and Women in Engineering Societies, National Interuniversity Consortium for Telecommunications (CNIT), and Italian Society of Electromagnetics (SIEm).